Spatial distributions of observables in systems under thermal gradients

Kenichiro Aoki[1,*] and Dimitri Kusnezov[2,†]
[1]*Department of Physics, Keio University, 4-1-1 Hiyoshi, Kouhoku-ku, Yokohama 223-8521, Japan*
[2]*Center for Theoretical Physics, Sloane Physics Lab, Yale University, New Haven, Connecticut 06520-8120, USA*
(Received 5 May 2004; published 22 November 2004)

Departures of observables from their thermal equilibrium expectation values are studied under heat flow in steady-state nonequilibrium environments. The relation between the spatial and temperature dependence of these nonequilibrium behaviors and the underlying statistical properties are clarified from general considerations. The predictions are then confirmed in direct numerical simulations within the Fermi-Pasta-Ulam β model. Nonequilibrium momentum distribution functions are also examined and characterized through their cumulants and the properties of higher order cumulants are discussed.

DOI: 10.1103/PhysRevE.70.051203 PACS number(s): 44.10.+i, 05.60.Cd, 63.10.+a, 11.10.Wx

I. INTRODUCTION

In studies of nonequilibrium physics, especially those of steady states, local equilibrium is most often invoked and this assumption simplifies calculations through the use of equilibrium statistical mechanics and thermodynamics [1]. The local equilibrium assumption allows the use of the equilibrium distribution function to compute observables. If local equilibrium conditions are not assumed, very little can be computed analytically and even the definition of temperature is no longer unique [2,3]. Efforts have been made to quantify the goodness of local equilibrium assumptions or how transport coefficients differ from their linear response values, though only few quantitative studies exist [4–11]. Without the knowledge of the nonequilibrium steady-state distribution, theoretical development becomes quite restrictive. We explore how observables depart from their equilibrium expectation values within a given nonequilibrium steady state, specifically focusing on the spatial dependence of the nonequilibrium expectation values within a given system and their local temperature dependence. To make this concrete, heat flow in the Fermi-Pasta-Ulam (FPU) β model is simulated to test the predictions. We further quantitatively examine the relationship between the momentum cumulants and the distribution and find that the lower order cumulants characterize the distribution quite well.

For systems in thermal gradients, it is natural to consider how an observable $\mathcal{O}$ in the nonequilibrium steady state departs from its equilibrium value, denoted $\mathcal{O}_{eq}$. The normalized deviation from equilibrium, when $\mathcal{O}_{eq}\neq 0$, can be expanded as

$$\delta_{\mathcal{O}} \equiv \frac{\delta\mathcal{O}}{\mathcal{O}} = \frac{\mathcal{O}-\mathcal{O}_{eq}}{\mathcal{O}_{eq}} = C_{\mathcal{O}}\left[\frac{\nabla T}{T}\right]^2 + C'_{\mathcal{O}}\left[\frac{\nabla T}{T}\right]^4 + \cdots . \tag{1}$$

When $\mathcal{O}_{eq}=0$, as is the case for higher order momentum cumulants, one can normalize by an observable which has the same dimensions. When local equilibrium is no longer valid, in general, no unique definition of temperature exists and a choice needs to be made. This definition of nonequilibrium temperature can be thought of as a choice of a coordinate system, on which the physics behavior of the system will not depend. If we assume analyticity in ∇T, the deviations $\delta_{\mathcal{O}}$ can be expanded in even powers as above. We shall see below that this expansion is adequate for describing the properties of the system.

The heat flow J is the flow of energy and can be unambiguously defined in Hamiltonian systems. Near equilibrium, it satisfies Fourier's law locally as $J=-\kappa\nabla T(x)$, where κ is the thermal conductivity, $T(x)$ is the temperature profile inside, and x is the position inside the system. In systems we consider, the energy flow is one dimensional and energy is put in or taken out only at the boundaries so that J does not depend on x. Fourier's law can then be used in Eq. (1) to re-express the local departures from equilibrium in terms of the temperature profile $T(x)$, or equivalently the position x once the coefficients C, C' are known,

$$\delta_{\mathcal{O}} = C_{\mathcal{O}}\left(\frac{J}{\kappa(T)T}\right)^2 + D'_{\mathcal{O}}\left(\frac{J}{\kappa(T)T}\right)^4 + \cdots . \tag{2}$$

We note that Fourier's law itself receives nonequilibrium corrections [11], which is why the coefficient of $\mathcal{O}(J^4)$ term in the expansion (2) differs from that of Eq. (1). In the following, the objectives will be to make the formula more explicit and understand its physical properties under rather general assumptions. This relation, together with $\kappa(T)$ [and consequently $T(x)$] provides the basis for defining how nonequilibrium observables vary inside a finite system both near and far from global thermal equilibrium.

II. FPU MODEL AND TEMPERATURE PROFILES

The results we present here are derived from general considerations and we develop them in conjunction with a model in which they can be explicitly analyzed. We study the FPU β Hamiltonian, defined generally in the form

*Email address: ken@phys-h.keio.ac.jp
†Email address: dimitri@mirage.physics.yale.edu

$$\tilde{H} = \sum_{k=0}^{L} \left[\frac{\tilde{p}_k^2}{2m} + \frac{1}{2} m\omega^2 (\tilde{q}_{k+1} - \tilde{q}_k)^2 + \frac{\beta}{4} (\tilde{q}_{k+1} - \tilde{q}_k)^4 \right]. \quad (3)$$

We use the FPU model since its physical properties are of wide interest (see Refs. [12–15] and references therein). Also as the model is well studied, we can understand the physical properties we find within a larger physics context. Under the rescaling $\tilde{p}_k = p'_k \omega^2 \sqrt{m^3}$, $\tilde{q}_k = q'_k \omega \sqrt{m}$, we obtain the conventional form of the FPU β model,

$$H_\beta = \frac{1}{2} \sum_{k=0}^{L} \left[p'^2_k + (q'_{k+1} - q'_k)^2 + \frac{\beta}{2} (q'_{k+1} - q'_k)^4 \right], \quad (4)$$

where $H_\beta = \tilde{H}/(m^2\omega^4)$. We note that in finite temperature simulations, changing the temperature is equivalent to changing the coupling β. Under the additional rescaling $p'_k = p_k/\sqrt{\beta}$, $q'_k = q_k/\sqrt{\beta}$, one obtains a unique, dimensionless, Hamiltonian $H \equiv H_{\beta=1} = \beta H_\beta$, which we shall use without any loss of generality. Since $p_k^2 = \beta p'^2_k$, the temperatures in the two formulations H and H_β are related by $T = \beta T'$.

In this work, we study the nonequilibrium steady state physics of the theory under thermal gradients, making use of nonequilibrium states constructed numerically. (For general discussion, see, for instance, Refs. [16,17].) The model is thermostatted at the boundaries $k = 0, L$ at various temperatures T_1^0, T_2^0, using the generalized versions of Nosé-Hoover thermostats as detailed in Ref. [18]. These additional thermostat degrees of freedom are added only at the boundaries and the degrees of freedom inside the system ($0 < k < L$) are exclusively those of the Hamiltonian Eq. (4). By numerically integrating the equations of motion of the whole system (including those of the thermostats), we obtain the behavior of physical observables in the non–equilibrium steady state by averaging over time, in the standard manner [17]. The local temperature at site k is defined as $T_k = \langle p_k^2 \rangle$. In this work, we study the physics inside the system, away from the boundaries by much more than the mean free path of the system [14]. The sensitivity of the results to the manner in which we apply the boundary conditions—including both the number of thermostats and the strength of the couplings—have been examined to ensure that physics results below remain independent of their implementation. (The only exceptions are the boundary jumps in temperature which we discuss below.) The numerical integrations were performed using the fourth order Runge-Kutta routines with time steps of $0.005 \sim 0.02$ for $10^7 - 10^{10}$ time steps. The equilibrium properties have been readily verified with this method [14,18].

In Fig. 1 some examples of temperature profiles for the FPU theory are shown. Generically, there are temperature jumps just inside the boundaries with smooth temperature variations within. The boundary jumps become larger as one moves away from global equilibrium. The jumps are dynamical in the sense that they depend on the model, the transport coefficient, heat flow, as well as the type of boundary conditions employed. The temperatures at the boundaries are at the thermostat temperatures to high degree of precision. For instance, in the examples of Fig. 1, the boundary

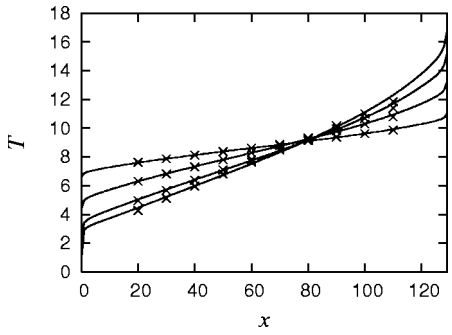

FIG. 1. Some examples of temperature profiles for the FPU model with $L = 128$. The thermostat temperatures at the boundaries are $(T_1^0, T_2^0) = (0.88, 16.72), (2.4, 15.2), (4.4, 13.2), (6.6, 11.0)$ for the four thermal profiles. The profiles predicted from Eq. (7) are indicated by $\times$ and agree well with the results from the numerical simulations.

temperatures are equal to the prescribed thermostat temperatures to within few in 10^5 relatively.

From temperature profiles and heat flow calculations, Fourier's law can be verified to hold up to corrections of the form (1), and the thermal conductivity κ can be obtained for a given temperature and system size. In the one-dimensional (1D) FPU model, κ depends on the system size L and does not display bulk behavior [13]. κ is also dependent on the temperature in a known manner [14]. Generally, in cases where we have a one-dimensional temperature gradient, the temperature profiles can be obtained by integrating Fourier's law as long as we are not too far from equilibrium [11,18,19]:

$$\int_{T_1}^{T(x)} \kappa(T) dT = -Jx, \quad J = -p_k[(q_{k+1} - q_k) + (q_{k+1} - q_k)^3]. \quad (5)$$

x is the continuum extrapolation of the discrete lattice index k. We note here that J is a constant within the system for a given set of temperature boundary conditions since there are no heat sinks or sources inside. T_1 in the integral is the temperature extrapolated to the boundary and is explained below.

In many situations, the temperature dependence of the thermal conductivity, within some temperature range, can be well described by

$$\kappa(T) = cT^{-\gamma}. \quad (6)$$

While this power law may not hold globally in T, it is often the case that it is sufficient for the region of interest, which is the case here. In such a situation, the temperature profile can be explicitly computed from Eq. (5) to be [18]

$$T(x) = \begin{cases} T_1 \left\{ 1 - \left[1 - \left(\frac{T_2}{T_1} \right)^{1-\gamma} \right] \frac{x}{L} \right\}^{1/(1-\gamma)}, & \gamma \neq 1 \\ T_1 \left(\frac{T_2}{T_1} \right)^{x/L}, & \gamma = 1. \end{cases} \quad (7)$$

Here, $T_{1,2}$ denote the boundary temperatures obtained by extrapolating the temperature profile inside the system and dif-

fers from the thermostat temperatures $T^0_{1,2}$ by the boundary temperature jumps. From Eqs. (5) and (6), the temperatures $T_{1,2}$ are found to obey a relation

$$-\frac{JL}{c} = \frac{T_2^{1-\gamma} - T_1^{1-\gamma}}{1-\gamma}. \tag{8}$$

To understand the temperature profile of the whole system, we further need an understanding of the temperature jumps at the boundaries [20]. Similar boundary slips have been seen in sheared systems and these effects have been known for a long time in real systems. To leading order, the temperature jumps can be described by (with n being the normal to the boundary)

$$|T_i - T_i^0| \simeq \frac{\alpha c}{L(1-\gamma)}[T_2^{1-\gamma} - T_1^{1-\gamma}] \sim \lambda \left| \frac{\partial T_i}{\partial n} \right| \quad (i = 1,2). \tag{9}$$

Here λ is the mean free path of the excitations, which for the FPU lattice model, is essentially the $\kappa(T)$ (up to a constant factor of order 1) due to kinetic theory arguments [14]. α reflects the efficacy of the boundary conditions. The last relation is obtained by using Fourier's law and Eq. (8). The jumps on the hot and cold side are the same provided the system is reasonably close to equilibrium. The jumps at the boundaries and the temperature profile within Eq. (7) describe the temperature profile of the complete system. The predicted values for the temperature profiles are plotted in Fig. 1 at a number points inside the systems ($\times$ symbols) away from the boundaries and are seen to be consistent with the simulation results. The thermal conductivity is roughly constant with respect to the temperature in this region so that $\gamma=0$ was used in the profile calculations. This demonstrates that all aspects of the nonequilibrium temperature profile can be quantitatively captured through Eqs. (7) and (9), irrespective of whether $\kappa(T)$ is a power law in temperature for all T or not. With this understanding of $T(x)$ we can now turn to the question of general observables.

III. SPATIAL DEPENDENCE OF CUMULANTS IN THE NONEQUILIBRIUM STEADY STATE

In nonequilibrium steady states, physical observables show deviations from their equilibrium values reflecting the lack of local equilibrium in the system. The behavior of the observables have been seen to be well described by Eq. (1) on average, at least in some cases [11]. Here, we now would like to investigate a more detailed issue—whether these properties can be used to understand the nature of the spatial profiles of these observables in a given nonequilibrium situation. We will assume that within some range of T and L that we can represent the expansion coefficients in Eq. (1) as

$$C_{\mathcal{O}} = \mu_{\mathcal{O}} T^{s_{\mathcal{O}}} L^{\alpha_{\mathcal{O}}}. \tag{10}$$

The behavior of $C_{\mathcal{O}}$ with respect to T,L clearly must depend on the dynamics of the theory and is not expected to be generic.

To study the spatial distribution of physical observables in nonequilibrium, we make use of Eq. (2) which describes how the observables should behave in nonequilibrium locally in space, given the thermal conductivity. Using this property and Eq. (6), we obtain to leading order that observables will deviate from their local equilibrium values as

$$\delta_{\mathcal{O}} = C_{\mathcal{O}} \left(\frac{JT(x)^{\gamma-1}}{c} \right)^2 = a_{\mathcal{O}} T(x)^{2(\gamma-1)+s}. \tag{11}$$

Here $a_{\mathcal{O}}$ is defined through this equation and should be proportional to J^2. This implicitly contains the spatial distribution since the temperature profile is known and can be understood as in Eq. (7).

While these arguments apply to any physical observable in the system, we choose to study cumulants of momenta p, mainly for the following reasons: conceptual and practical. There seems to be no universal rigorous definition of local equilibrium, yet the concept in the least seems to include a unique meaning for temperature, which in this case would lead to the Maxwellian distribution for p. To put it another way, when the momentum distribution is not Maxwellian, we can choose different definitions of the temperature based on the various moments of p [2,3]. The cumulants of the momentum distribution provide insight into how the physical properties of a nonequilibrium system deviates from those of local equilibrium. The cumulants are well defined local variables and their values in local equilibrium are known precisely. The low order cumulants are defined as

$$\langle\langle p^2\rangle\rangle = \langle p^2\rangle, \quad \langle\langle p^4\rangle\rangle = \langle p^4\rangle - 3\langle p^2\rangle^2,$$

$$\langle\langle p^6\rangle\rangle = \langle p^6\rangle - 15\langle p^2\rangle\langle p^4\rangle + 30\langle p^2\rangle^3, \ldots, \tag{12}$$

where, in *equilibrium*,

$$\langle\langle p^2\rangle\rangle_{eq} = T, \quad \langle\langle p^n\rangle\rangle_{eq} = 0 \ (n \neq 2). \tag{13}$$

This property is also of practical importance. Since the deviations we compute can be small, it is desirable to use observables whose local equilibrium values are known exactly. In this case in thermal equilibrium, $\mathcal{O}_{eq}=0$, so we use $\delta_{\mathcal{O}} = \langle\langle p^{2n}\rangle\rangle / T^n$. We list the coefficient for the case $\mathcal{O}=\langle\langle p^4\rangle\rangle$ in Table I for the FPU β model as well as ϕ^4 theory [18] for comparison.

Let us investigate how well Eq. (11) describes the spatial distribution of $\langle\langle p^4\rangle\rangle / T^2$. We find

$$\frac{\langle\langle p^4\rangle\rangle}{T^2} = a_4 T^{2(\gamma-1)+s_4} = a_4 \left(T_1 \left\{ 1 - \left[1 - \left(\frac{T_2}{T_1} \right)^{1-\gamma} \right] \frac{x}{L} \right\}^{1/(1-\gamma)} \right)^{2(\gamma-1)+s_4}. \tag{14}$$

s_4 is the temperature dependence of the coefficient C_4 which is reflected in Table I. To understand the validity of the prediction Eq. (14) , fits were made with just one parameter a_4 for the whole profile. We find that this describes the situation quite well, as seen in the examples of Fig. 2, where the predictions are denoted by dashes. In these figures, we have compared the fits with the spatial as well temperature dependence of $\langle\langle p^4\rangle\rangle$ for the four systems shown in Fig. 1. In this temperature range, temperature dependence of the thermal

TABLE I. Nonequilibrium coefficients $C_4=(\mu T^s)L^\alpha$ for $\langle\langle p^4\rangle\rangle/T^2$ [cf. Eqs. (10) and (14)]. The results are shown for the FPU β model and the ϕ^4 theory in $d=1-3$ dimensions. The value of s is extracted from fitting to several temperatures.

		(μT^s)	α
FPU β model in $d=1$			
$T=1$		29(5)	0.87(4)
$T=8.8$		13(1)	0.99(1)
$T=88$		7.4(4)	1.04(2)
ϕ^4theory			
$d=1$	$T=1$	3.3(24)	0.96(15)
	$T=5$	1.6(6)	1.18(9)
$d=2$	$T=1$	1.9(4)	1.09(5)
	$T=5$	0.4(2)	1.6(2)
$d=3$	$T=1$	4 (1)	0.96(10)
	$T=5$	0.2(5)	1.6(6)

conductivity is weak so we used $\gamma=0$ and $s_4=-0.14$ extracted from the data in Table I. Similar results were found for different temperature boundary conditions and for different L. To further verify the underlying physics, we study the J dependence of the coefficient a_4. The behavior for various systems, including the four systems in Fig. 1, are shown in Fig. 3. Each data point represents a system with a particular size and temperature boundary conditions. The central temperature is around $T=8.8$ and is kept fixed. The observed

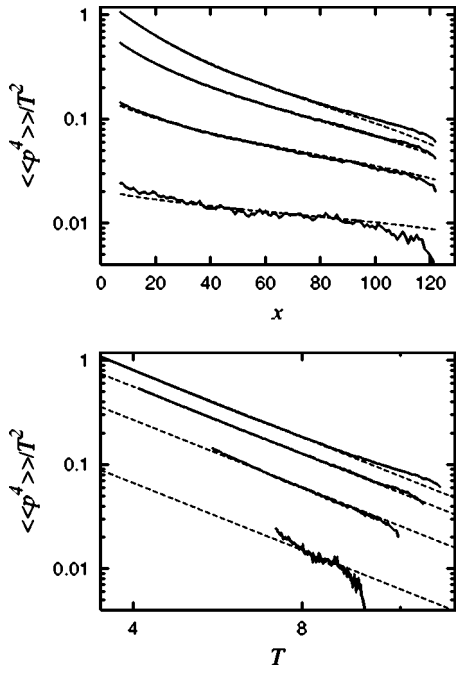

FIG. 2. Top: Spatial dependence of the rescaled fourth momentum cumulant, $\langle\langle p^4\rangle\rangle/T^2$ for the four systems in Fig. 1. Larger cumulant values are seen for larger boundary temperature differences. Bottom: Temperature dependence of $\langle\langle p^4\rangle\rangle/T^2$ for the same systems. In both panels, the predictions Eq. (11) are indicated by the dashes.

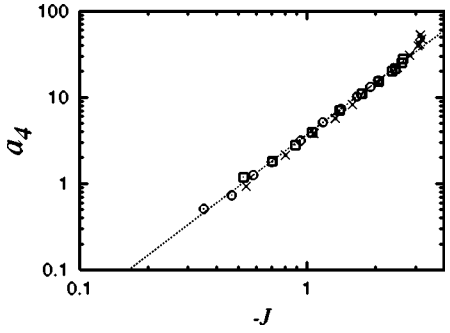

FIG. 3. J dependence of the nonequilibrium expansion coefficient a_4 for various boundary conditions (T_1^0, T_2^0) and system sizes L. The dashed line is $3.72\ J^2$ and the $\sim J^2$ behavior of the coefficient can be clearly seen, as predicted from theory. Each data point represents a particular temperature boundary condition for $L=32$ (×), $L=64$ (□), and $L=128$ (○) systems.

behavior is clearly well described by $a_4 \sim \text{const} \times J^2$. The coefficient a_4 seems L independent and this can roughly be understood since c^2 grows in L in a manner similar to C_4. We have in addition systematically studied the results to see if we can discern the contribution of higher order terms in the expansions (1), (2) (of order J^4 and higher) but have found no consistent evidence for them. In other physical situations, nonanalytic behavior seems to have been seen in some cases [21,22].

While the logic seems to work for the lowest nontrivial order cumulant, $\langle\langle p^4\rangle\rangle$, we find it instructive to analyze if it works at higher orders. In this direction, we have analyzed the next nontrivial order $\langle\langle p^6\rangle\rangle$ and have found that its behavior is quite consistent with physics of Eq. (11) , as was the case of $\langle\langle p^4\rangle\rangle$, in all the systems we have studied. In practice, higher order cumulants are more prone to errors and the computations are more difficult. The results for the same four systems in Fig. 1 are shown in Fig. 4. As in the $\langle\langle p^4\rangle\rangle$ case, the coefficient a_6 shows J^2 behavior within error, as it should. a_6 shows a weak L dependence, as we would generically expect. A common value of $s_6=-1.6$ was adopted for all the data in Figs. 4 and 5. What is evident is that the spatial behavior of nonequilibrium observables can be explicitly related to transport and other physical properties of the system using rather general considerations. From the cumulants we now consider what can be said about the full momentum distribution function.

IV. CUMULANTS AND THE DISTRIBUTION

The cumulants are quantitative indicators of the non-Maxwellian nature of the momentum distribution or the violations of local equilibrium. All the cumulants are nonzero unless the system is in local equilibrium, in which case only the linear and quadratic cumulants are nonzero. There are very few problems where cumulants can all be computed analytically and it becomes numerically intractable to compute them as we go to higher orders. It is then of interest to see how well the lower order cumulants characterize the distribution. The cumulants are properties of the distribution

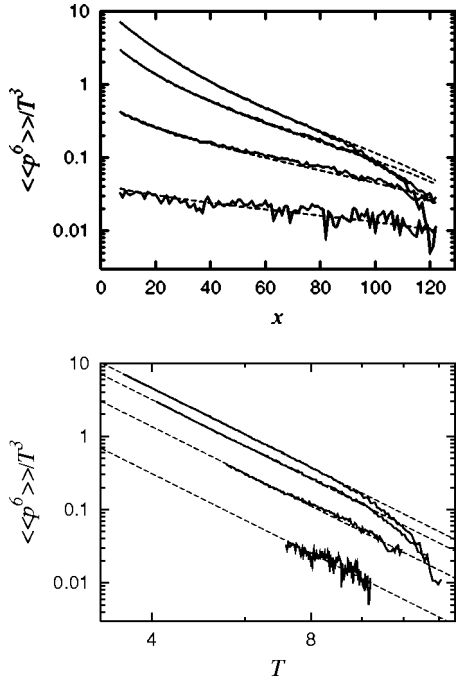

FIG. 4. Spatial dependence (top) and temperature dependence (bottom) of $\langle\langle p^6\rangle\rangle/T^3$ for the four systems in Fig. 1. Larger cumulant values are seen for larger boundary temperature differences. Predictions are shown with dashes.

function, which has an infinite number of degrees of freedom. *A priori*, there is no reason to assume that the lower order cumulants characterize the distribution. In order to clarify this issue, first note that the distribution function $f(p)$ and the cumulants are related explicitly through the generating function as

$$\int dp\ e^{iup} f(p) = \langle e^{iup}\rangle = \exp\left(\sum_{n=0}^{\infty} \frac{i^n u^n}{n!}\langle\langle p^n\rangle\rangle\right) = \exp\left(\sum_{n=0}^{\infty} \frac{(-u^2)^n}{(2n)!}\langle\langle p^{2n}\rangle\rangle\right). \quad (15)$$

Here, in the last equality, the symmetry under $p \leftrightarrow -p$ was used, which leads to $\langle\langle p^{2n+1}\rangle\rangle = 0$. We see from this equation that given all the cumulants (or equivalently, moments), we may recover the distribution function by performing an inverse Fourier transform. However, in practice, not all the cumulants are available.

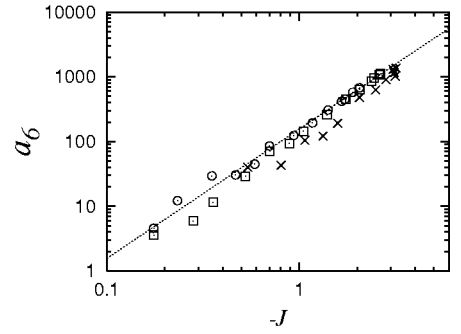

FIG. 5. J dependence of the coefficient a_6 for various boundary conditions (T_1^0, T_2^0) and system sizes L. The dashed line denotes $156\,J^2$. $\sim J^2$ dependence of a_6 is evident, in agreement with the predictions. Each data point represents a particular temperature boundary condition for system sizes $L=32$ (×), $L=64$ (□), and $L=128$ (○), as in Fig. 3.

It might seem that the symmetry under the reflection $q,p \leftrightarrow -q,-p$ (lattice indices suppressed here to avoid cluttering the formulas) is broken by the boundary conditions of the system, which are asymmetric in the direction of the lattice. However, this is *not* so; the reflection $q,p \leftrightarrow -q,-p$ is preserved under the boundary conditions since the degrees of freedom q,p are not directly related to the spatial direction of the lattice. This can be explicitly seen by checking that the equations of motion preserve this symmetry. It should be noted that J defined in Eq. (5) is symmetric under this reflection and that it is rather the correlations of q and p that are nonzero, not individual q,p's. In practice, the odd moments $\langle p^{2n+1}\rangle$ are computed in all our simulations at least up to seventh order, in some cases up to 19th order. We have checked that they are always zero within statistical errors.

Intuitively, we expect the lower order cumulants to be the leading order results with higher order cumulants becoming more important as we move further away from equilibrium. In Fig. 6, we plot the *relative difference* of the measured distribution $f(p)$ to the thermal distribution $f_0(p)$ for the distribution directly measured in the simulations and the distribution computed from the low order cumulants $\langle\langle p^{2,4,6}\rangle\rangle$. The comparisons are performed for the four systems in Fig. 1 at a point in the middle of the system. From these graphs, we observe the following: (a) The agreement between the distribution computed from lower order cumulants and the distribution is quite good in all cases; (b) the relative deviation from the thermal distribution is larger as we move away from equilibrium (larger $\Delta T/T$), as expected; (c) the small discrepancy between the computed distribution and the measured one seems to be larger for larger $\Delta T/T$; (d) the deviation from the thermal distribution becomes more noisy for smaller $\Delta T/T$, since the deviation itself is smaller and the relative error is larger. We mention here that strictly speaking, the distributions can have different behavior, such as long tails, beyond the region we have investigated. However, these tails would have to be quite small since the distributions decay as $\exp[-p^2/(2T)]$ and the agreement is good up to reasonably large p, as seen in Fig. 6. We have examined numerous systems for different T and L and found similar good agreement. Therefore we see that the lower order cumulants provide good physical observables that quantitatively describe the deviations of the systems from local equilibrium, at least in the FPU model.

It is possible to examine the characteristics of the higher order cumulants. It should be noted that unlike the even moments $\langle p^{2n}\rangle$, even cumulants, $\langle\langle p^{2n}\rangle\rangle$, need not be positive and in general will not be. So to study the general trend of the cumulants for higher order, we examine the magnitude of the cumulants. In Fig. 7 (left), we show the behavior of the cumulants up to 20th order for the same four systems in Fig. 1, specifically for the point at which the momentum distributions in Fig. 6 were computed. Only data points with reasonable error are shown and an explanation of the relevant errors

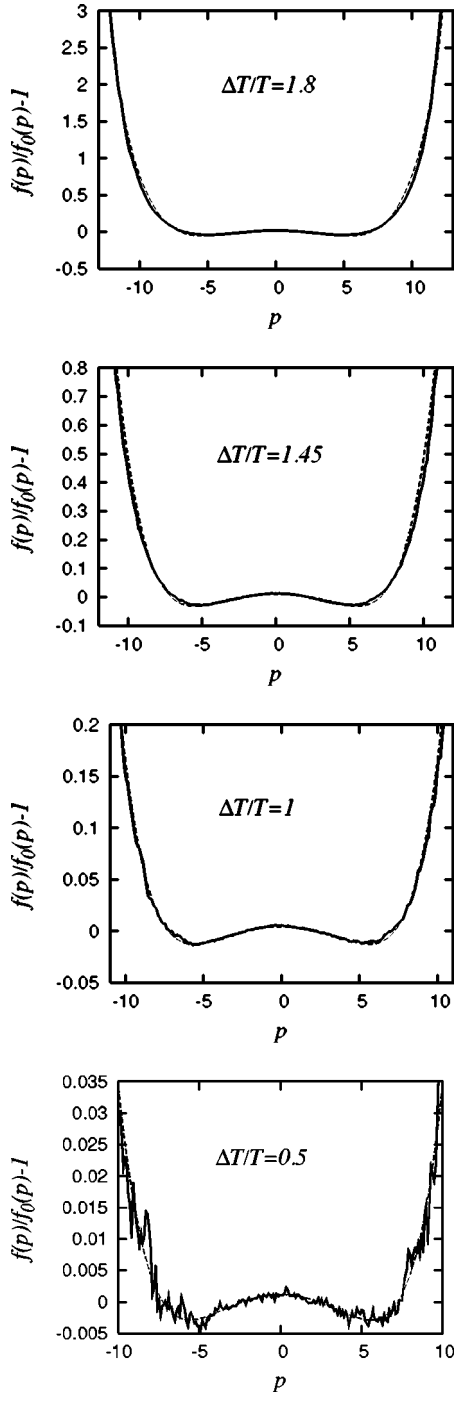

FIG. 6. The relative deviation of the distribution from the Maxwell distribution for the four systems in Fig. 1. Distribution obtained from the cumulants $\langle\langle p^4\rangle\rangle, \langle\langle p^6\rangle\rangle$ (dashed) are compared with the measured distributions (solid). The agreement is excellent. $\Delta T/T$ denotes the boundary temperature difference over the average temperature and is an indication of how far the system is from equilibrium.

is given below. We see an increase in the magnitude with the order is roughly exponential. This growth is far milder than the $(2n)!$ seen in Eq. (15) .

The behavior of the higher order cumulants is of some import and we briefly explain semiquantitatively why they

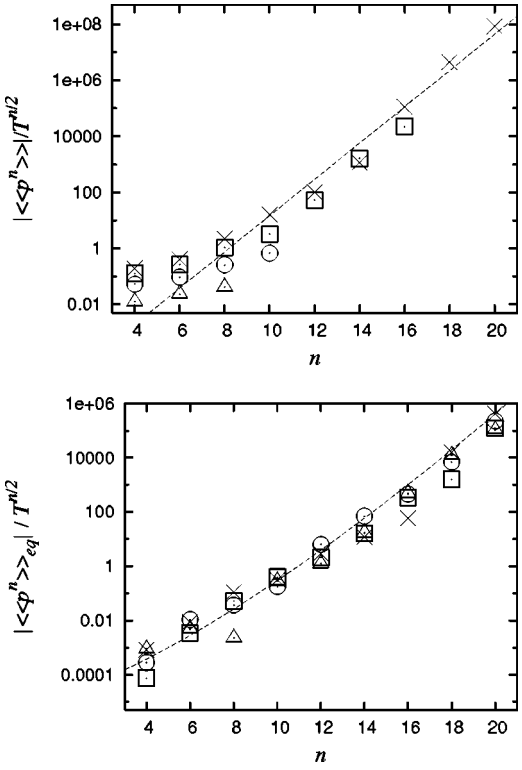

FIG. 7. (top) Higher order cumulants, $|\langle\langle p^n\rangle\rangle|/T^{n/2}$ $(n \leqslant 20)$ for the four systems in Fig. 1, $(T_1^0, T_2^0) = (0.88, 16.72)$, $(\times)$, $(2.4, 15.2)$, $(\square)$, $(4.4, 13.2)$, $(\bigcirc)$ and $(6.6, 11.0)$, $(\triangle)$. Only points with reasonably small error are shown. The dashed line is $5.0 \times 10^{-6} \exp(1.5n)$ drawn for comparison. (bottom) The equilibrium cumulants for $L=16$ $(\times)$, $L=32$ $(\square)$, $L=64$ $(\triangle)$ and $L=128$ $(\bigcirc)$ compared to the rough estimate, Eq. (18) (dashes). The cumulants $\langle\langle p^2\rangle\rangle$ were measured at the middle of the system with number of samples $N=10^9$ at $T=8.8$.

are difficult to obtain. The difficulty lies mainly in the statistical error in the simulations. This can be estimated from the number of samples for computing the expectation values as

$$\frac{\Delta\langle p^n\rangle}{\langle p^n\rangle} \sim \frac{n}{\sqrt{N}}, \tag{16}$$

where Δ denotes the error and N is the total number of samples or the number of time steps in the simulation. Note that $\langle\langle p^n\rangle\rangle = \langle p^n\rangle + \cdots$ so that an error estimate for the moment should suffice as the error estimate for the cumulant. An adequate value for the moment can be obtained in equilibrium,

$$\frac{\langle p^n\rangle}{T^{n/2}} \sim (n-1)\,!!\,. \tag{17}$$

Combining these relations, we find the statistical error for the cumulants which increases rapidly for higher order cumulants,

$$\Delta\left(\frac{\langle\langle p^n\rangle\rangle}{T^{n/2}}\right) \sim \frac{(n-1)\,!!\,n}{\sqrt{N}}. \tag{18}$$

These estimates for the error also apply to the equilibrium situation. In contrast to the nonequilibrium cumulants, the equilibrium cumulants should vanish, with the exception of $\langle\langle p^2\rangle\rangle$. As the measured values will converge to zero, at any given time step in the simulation, their values will be generically nonzero. In Fig. 7 (right), we compare the *equilibrium* cumulants, in the middle of the system to the above error estimates. It can be seen that the rough estimate (18) seems to be consistent with the results. As one samples more (N increases), these will tend to zero. However, for a finite sample size, this is found to explain the order of the uncertainty.

With $N=10^9$ time steps—which we used for the values in Fig. 7—for eighth and tenth order cumulants, the errors are 0.03 and 0.3. As we can see from Fig. 7 (left), this means that we can obtain up to the eighth or tenth cumulant with reasonable error for the four systems but the higher order cumulants are expected to be unreliable for systems closer to equilibrium. These error estimates are quite consistent with the estimates we obtain from the statistical properties of the simulations. These errors can be overcome with higher statistics which quickly becomes unrealistic for higher order. We have analyzed systems with various other temperature boundary conditions and L and have found the increasing behavior of the cumulants seen in Fig. 7 (left) to be quite generic.

V. SUMMARY AND DISCUSSIONS

The spatial distribution of cumulants in nonequilibrium steady states under thermal gradients were predicted from general considerations and tested in the FPU model. The understanding of the temperature profile for a given nonequilibrium steady state, combined with the deviations of physical observables from their equilibrium values, can be used to develop a consistent description of the spatial distribution of observables. In principle, the behavior of observables probably have higher order corrections in the nonequilibrium nature of the system, which in this case is ∇T, but higher order effects could not be separated within the current numerical simulation results.

We quantitatively analyzed the relation between the momentum cumulants and the distribution in the nonequilibrium steady state. It was found that the lower order cumulants characterize the difference of the nonequilibrium distribution from the one in local equilibrium quite well. Understanding and characterizing the properties of the distribution is of manifest importance since the distribution function for physical variables allows us to compute *any* observable constructed from these variables. To understand the properties of any local variable in the nonequilibrium state, the physical properties of the coordinate variables also need to to be clarified. We have also computed some behavior of higher cumulants. The expansion of the nonequilibrium distribution function in terms of cumulants has similarities to Grad's method in kinetic theory [1]. Grad proposed an ansatz for the nonequilibrium solution to Boltzmann's equation by expanding around the equilibrium distribution in terms of moments of the molecular velocity. Such a moment expansion has similarities to the cumulant expansion since the cumulants can be related to the moments. Grad's approach takes as an ansatz a finite moment truncation and uses a transport equation to determine the coefficients in the expansion. In our study, we extract each cumulant independently from a direct measurement and do not use a transport equation approach. Since the moments can be computed from the cumulants and we find that the few leading cumulants reproduce the steady-state solution quite well, it would be interesting to see how a Grad solution might be related and explore how a Boltzmann-type approach might be used to understand states far from equilibrium, as compared to the direct microscopic molecular dynamics solutions employed here.

The notion of temperature in nonequilibrium simulations is unambiguous as long as we adopt a particular definition of the temperature. In our analysis, we adopted a kinetic temperature, the ideal gas temperature, as such a definition. The differences in temperature due to various definitions are measures of deviations from local equilibrium. Seen in this light, we can understand the nonzero cumulants computed above as the discrepancy between temperatures defined from the various moments of p. Other natural definitions of temperature, such as "configurational temperature" based on the potential, or that based on the energy density, involve the potential energy (for recent discussions, see, for instance, Refs. [23] and [18]). In lattice models, definitions of temperature that involve the potential are subtle, since they are, strictly speaking, neither unique nor local because the potential necessarily couples different sites. It would be interesting to compare these temperatures with the kinetic one in the FPU model.

A comment is perhaps in order: lack of local equilibrium behavior can in some cases be attributed to the lack of coarse graining [4]. Heuristically speaking, if one does not have a large number of degrees of freedom, one cannot see the equilibrium behavior. This is a *different* phenomenon from the case at hand, since the effective number of degrees of freedom is the number of samples in the ensemble average which is taken in the time averaging procedure. This number is huge. In fact, as is well known, in these types of ensembles, it makes perfect sense to talk even about the statistical mechanics of one spin degrees of freedom. This is also quite clear from our results; the deviations from local equilibrium seen in Figs. 2 and 4 and Eq. (2) are of definite sign and no amount of averaging over space will make it zero. So coarse graining will *not* average out the violations of local equilibrium seen above. Also, the non-local equilibrium properties found in this paper pertain to systems in the nonequilibrium steady state and therefore are not transient.

We have also performed similar analyses of spatial distributions on the ϕ^4 model. The physical properties of the model are different from those of FPU model and we intend to report on this in the near future.

ACKNOWLEDGMENT

K.A. was supported in part by a Grant-in-Aid from the Ministry of Education, Science, Sports and Culture.

[1] See, e.g., S. R. de Groot and P. Mazur, *Non-equilibrium Thermodynamics* (North-Holland, Amsterdam, 1962); D. Jou, G. Lebon, and J. Casas-Vazques, *Extended Irreversible Thermodynamics* (Springer, Berlin, 1996).
[2] J. Keizer, *Statistical Thermodynamics of Nonequilibrium Processes* (Springer, New York, 1987).
[3] J. Casas-Vazquez and D. Jou, Rep. Prog. Phys. **66**, 1937 (2003), and references therein.
[4] A. Tenenbaum, G. Ciccotti, and R. Gallico, Phys. Rev. A **25**, 2778 (1982).
[5] G. Ciccotti and A. Tenenbaum, J. Stat. Phys. **23**, 767 (1980); C. Trozzi and G. Ciccotti, Phys. Rev. A **29**, 916 (1984).
[6] B. Hafskjold and S. K. Ratkje, J. Stat. Phys. **78**, 463 (1995).
[7] W. Loose and G. Ciccotti, Phys. Rev. A **45**, 3859 (1992); M. Mareschal, E. Kestemont, F. Baras, E. Clementi, and G. Nicolis, *ibid.* **35**, 3883 (1987); A. Tenenbaum, *ibid.* **28**, 3132 (1983).
[8] R. M. Valesco and L. S. Garcia-Colin, J. Non-Equilib. Thermodyn. **18**, 157 (1993).
[9] A. Dhar and D. Dhar, Phys. Rev. Lett. **82**, 480 (1999).
[10] S. Takesue, Phys. Rev. Lett. **64**, 252 (1990).
[11] K. Aoki and D. Kusnezov, Phys. Lett. A **309**, 377 (2003).
[12] H. Kaburaki and M. Machida, Phys. Lett. A **181**, 85 (1993); A. Maeda and T. Munakata, Phys. Rev. E **52**, 234 (1995).
[13] S. Lepri, R. Livi, and A. Politi, Phys. Rev. Lett. **78**, 1896 (1997); Europhys. Lett. **43**, 271 (1998).
[14] K. Aoki and D. Kusnezov, Phys. Rev. Lett. **86**, 4029 (2001).
[15] J. Ford, Phys. Rep. **213**, 271 (1992); S. Lepri, R. Livi, and A. Politi, *ibid.* **377**, 1 (2003).
[16] P. Gaspard, *Chaos, Scattering and Statistical Mechanics* (Cambridge University Press, New York, 1998); J. R. Dorfman, *An Introduction to Chaos in Nonequilibrium Statistical Mechanics* (Cambridge University Press, Cambridge, England 1999).
[17] D. J. Evans and G. P. Morriss, *Statistical Mechanics of Nonequilibrium Liquids* (Academic, New York, 1990); W. G. Hoover, *Computational Statistical Mechanics* (Elsevier, Amsterdam, 1991); *Time Reversibility, Computer Simulation, and Chaos* (World Scientific, Singapore, 1999); Ann. Phys. (N.Y.) **295**, 50 (2002)
[18] K. Aoki and D. Kusnezov, Ann. Phys. (N.Y.) **295**, 50 (2002); Phys. Lett. B **477**, 348 (2000).
[19] C. S. Kim and J. W. Dufty, Phys. Rev. A **40**, 6723 (1989); N. Nishiguchi, Y. Kawada, and T. Sakuma, J. Phys.: Condens. Matter **4**, 10227 (1992).
[20] K. Aoki and D. Kusnezov, Phys. Lett. A **265**, 250 (2000).
[21] G. Marcelli, B. D. Todd, and R. J. Sadus, Phys. Rev. E **63**, 021204 (2001); J. P. Ryckaert, A. Bellemans, G. Ciccotti, and G. V. Paolini, Phys. Rev. Lett. **60**, 128 (1988); S. Rastogi, N. Wagner, and S. Lustig, J. Chem. Phys. **104**, 9234 (1996); D. Evans and H. J. M. Hanley, Phys. Lett. **80A**, 175 (1980).
[22] K. Kawasaki and J. D. Gunton, Phys. Rev. A **8**, 2048 (1973); H. Wada and S. Sasa, Phys. Rev. E **67**, 065302(R) (2003).
[23] A. Baranyai, Phys. Rev. E **61**, R3306 (2000); T. Hatano and D. Jou, *ibid.* **67**, 026121 (2003).